CSCE Annual Conference

Growing with youth – Croître avec les jeunes

Laval (Greater Montreal)

June 12 - 15, 2019

EFFECT OF CHANGING BOUNDARY ELEMENT SIZE ON THE RESPONSE OF REINFORCED CONCRETE MASONRY SHEAR WALLS WITH C-SHAPE BOUNDARY ELEMENT

Albutainy, Mohammed[1]
[1] Concordia University, Canada
m_albuta@encs.concordia.ca

Galal, Khaled[2]
[2] Concordia University, Canada
khaled.galal@concordia.ca

Abstract: New ductile reinforced masonry shear walls (RMSW) category with a seismic ductility-related force modification factor, Rd, of 3.0 was introduced in the current Canadian National Building Code and masonry design standards. Consequently, this promotes RMSW as a potential seismic force resisting system (SFRS) alternative in mid-rise buildings. One way of increasing reinforced masonry shear walls curvature and displacement ductility is by adding confined boundary elements to the walls' end zones to enhance the ultimate compressive strain and wall curvature ductility. The boundary elements in the previously tested walls were constructed using regular stretcher blocks. Using regular stretcher blocks caused some limitations due to the geometry restrictions of the stretcher units. This paper reports results of two of six half-scale RM walls with boundary elements specimens that were tested under a reversed cyclic moment and lateral loading. New boundary element block (i.e. C-shaped blocks) were utilized to form the boundary elements in the tested walls to overcome the limitations that arise from using stretched units. These walls represent the plastic hinge zone located in the lower one-and-a-half story of a +10-story RM shear wall building. The wall's boundary elements are varied in size as well as vertical and transverse reinforcement ratios. The paper presents the experimental work and focuses on quantifying the effect of changing the boundary element size on wall's lateral capacity, ductility ratio, maximum compressive strain, in-plane mode of failure, amount of dissipated energy and damping ratio.

1 INTRODUCTION

Reinforced masonry shear walls (RMSW) have been proved, through testing, to be able to provide the required strength and ductility for being considered as an efficient lateral resisting system in buildings. Recent research efforts toward enhancing the design of RM walls are reflected in the current CSA S304-14 and the NBCC 2015 (Canadian Commission on Building and Fire Codes 2015), by introducing a new ductile RM wall with lateral force reduction factor (R_d) of 3.0. Hence, reinforced concrete masonry shear walls could be considered as a sufficient lateral force resesting system for mid-rise buildings. Researchers studied the effect of vertical and horizontal reinforcement ratio, axial load, and wall aspect ratio (height to length ratio) on the lateral response of reinforced masonry shear walls. Shedid et al. (2010) tested seven

RMSW with three different end configurations (rectangular, flanged, and end-confined). The results showed that using flanged and confined boundary element increased wall's ductility by 39% and 106% respectively when compared with rectangular walls. Oh et al. (2002) tested 4 reinforced concrete shear walls to investigate the effect of changing boundary elements detailing on the shear wall's deformation capacity. Oh et al. concluded that increasing the confinement in the boundary elements can increase the deformation capacity of the wall significantly. Also, changing the wall cross section from rectangular to bell shape while keeping the same vertical and transvers reinforcement ratio in the boundary elements has a minor effect on the wall response (Oh, Han, and Lee 2002). Kapoi 2012 tested eight full-scale uncontained RMSW and studied the effect of concentrated reinforcement on the end zones of the masonry walls. Kapoi concluded that the performance of the evenly distributed reinforcement wall was very similar to that of walls with concentrated reinforcement of the ductility of the displacement. Walls with concentrated reinforcement, however, found that 50% more energy was dissipated. Previously tested RMSW with boundary elements are limited in the literature. The boundary elements in these tested walls were made from regular stretcher blocks, except one wall tested by Shedid et al. (Shedid., and El Dakhakhni, 2010). Using stretcher masonry units restricts the boundary elements shape to the square and restricts the number of vertical reinforcement bars. Moreover, using stretcher units without doing the extensive cutting to reshape the unit does not provide the required vertical reinforcement buckling prevention spacing.

This study utilized a new boundary element block (i.e., similar to available pilaster blocks but with different dimensions) to build RMSW with end confined boundary elements. Here the boundary element is formed using two C-shape masonry units facing each other and the steel cage is installed as one piece. C-shaped BE has the advantage of providing more homogenous grouted core, flexibility in selecting boundary element size and amount of vertical and transverse reinforcement. This new boundary element block eliminates the limitations associated with regular concrete blocks (i.e., stretchers) utilized in previous studies (Shedid, Dakhakhni, 2010, Banting and El-Dakhakhni 2012). The configuration of the new boundary was achieved in collaboration with the masonry industry partners in Canada.

2 EXPERIMENTAL PROGRAM

Six half-scale fully grouted reinforced masonry shear walls were built and tested under reversed cyclic lateral load and top moment in two phases. The specimens represent the plastic hinge zone located in the lower story panel of 12-story reinforced masonry shear wall building. C-shape masonry units were used to construct the boundary elements instead of the stretcher units. The wall's boundary elements are varied in size and vertical and transverse reinforcement ratios. All walls were designed to be flexure dominated. Shear walls were designed to provide shear and sliding resistance with a safe margin to avoid undesirable shear failure. Deformed wires shear reinforcement D8 (diameter = 8.11 mm) with 90°/180° hook spaced at 285 mm along the height of the wall were placed alternatively (Robazza et al. 2013). Also, D8 horizontal reinforcement bars with 180° hooks were embedded in the boundary element and extended inside the web with sufficient development length to resist the shear flow between boundary element and the web.

2.1 Details of specimens

One of the advantages of using C-shaped masonry units to form the boundary elements that it could give the flexibility to change the shape and the size of the boundary element. Wall 4 and wall 5 were designed to have the same lateral resistance to investigate the effect of changing the boundary element size on the seismic response of the masonry shear wall. Both walls were designed to have almost the same total length and the lateral capacity. Table 1 shows a summary of wall details. l_b and b_b are the length and the width of the boundary elements respectively. ρ_v is the vertical reinforcement ratio in the boundary elements. l_w and b_w are the length and thickness of the web, respectively. Walls reinforcement details are shown in Figure 1.

Table 1. Wall's lateral strength

Wall	Boundary Element					Web			
	L_b (mm)	b_b (mm)	ρ_v (%)	Vert. Reinf.	Hoops size@spacing	L_w (mm)	b_w (mm)	Vert. Reinf.	Hori. Reinf.
Wall 4	190	190	1.57	8#3	D4@60 mm	1335	90	4#3	D8@190 mm
Wall 5	290	190	1.03	8#3	D4@60 mm	1145	90	4#3	D8@190 mm

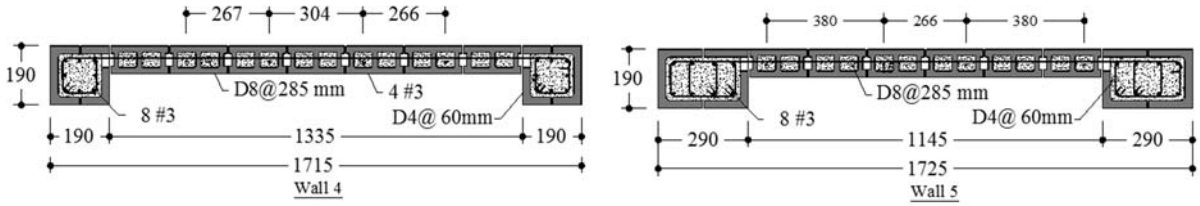

Figure 1: Walls reinforcement details.

2.2 Material prosperities

Ready-to-use type S mortar was used to construct both walls. The average compressive strength of eight 50x50x50mm mortar cubes is 19.1MPa (c.o.v= 9.48%). Two types of fine grout mixes were used for grouting the walls. The first type is high strength grout used in in the boundary elements and the second type is normal strength grout used in the web area. The average compressive strength of six grout cylinders was 28 MPa (c.o.v. = 13.3%) and 43.3 MPa (c.o.v. = 14.8%) for high and normal strength grout respectively. Five fully grouted 4-blocks high boundary elements prisms were constructed using C-shaped block units. The average compressive strength of the boundary elements prisms, f_m, was 23.7 MPa (c.o.v. = 11.3%). Five fully grouted 4-blocks high prisms were constructed in running bond to obtain the compressive strength of the web area. The average compressive strength of the web prisms, f_m, was 10.20 MPa (c.o.v. = 5.8%). The yield and ultimate strength of #3 vertical bars found to be 460 MPa and 680 MPa respectively. The yield and ultimate strength of D4 bars determined from the tensile test were 588 MPa and 633 MPa respectively.

2.3 Test set-up and procedure

Tests were conducted using a specialized test setup steel frame equipped with three actuators for load application. The test setup allows the application of displacement increments in a quasi-static pattern to observe walls full lateral behaviour. The reaction frame shown in Figure 2 is designed to support two vertical and one horizontal actuator. The capacity of each of the three MTS digitally-controlled actuators is 750 kN in compression and tension with a maximum stroke of 400 mm. The test setup allows testing shear wall's plastic hinge zone panels when subjected to constant axial load along with synchronized cyclic top moment applied by the vertical actuators along with the lateral cyclic displacement applied by the horizontal actuator. The laboratory's strong floor has six tie-down pairs of anchorages. Heavily reinforced concrete pad (transfer footing) was constructed to tie specimen footing to the laboratory's strong floor. The transfer footing is secured to the strong floor via twelve 2" high-strength threaded rods to prevent sliding and overturning of the specimens. Wall footing is a 2300×640×400 mm reinforced concrete footing. This foundation was secured to the base foundation by eighteen (out of available forty-four) 1" high tensile threaded rods. The relative displacements were monitored in two locations using linear potentiometers: between the wall and the top loading beam, and between the wall and the wall's footing, were measured using a linear potentiometer in order to capture any sliding that may occur either at the top or at the bottom of the wall. The uplift of the wall's footing was measured using string potentiometer to include the effect of uplift on the lateral displacement (if any). The test measurements show that there was no sliding nor uplift.

The out-of-plane support was provided in two levels, the floor level and the actuator level. W250x45 steel beams were used. Three screw jacks were installed on each side between the wall and the steel beams. Teflon plates were installed on the top concrete loading beam and the masonry wall at the first-floor level in order to ensure that there is no friction between the screw jacks and the specimen.

Six string potentiometers were attached to rigid support from one side, and the other side they were attached to the specimen to measure the lateral displacement and the sliding of the wall. Twelve LVDT's were mounted on the wall ends to measure wall curvature. Relative displacement between the web and boundary elements; and web and top and bottom footings also were measured by LVDT's. Finally, shear deformation was tracked by two potentiometers mounted in a cross shape along with the panel height. Twenty strain gauges were installed on the outermost bars in each wall to capture the yield initiation and propagation over the loading history. Footing uplift and sliding were monitored using string potentiometers.

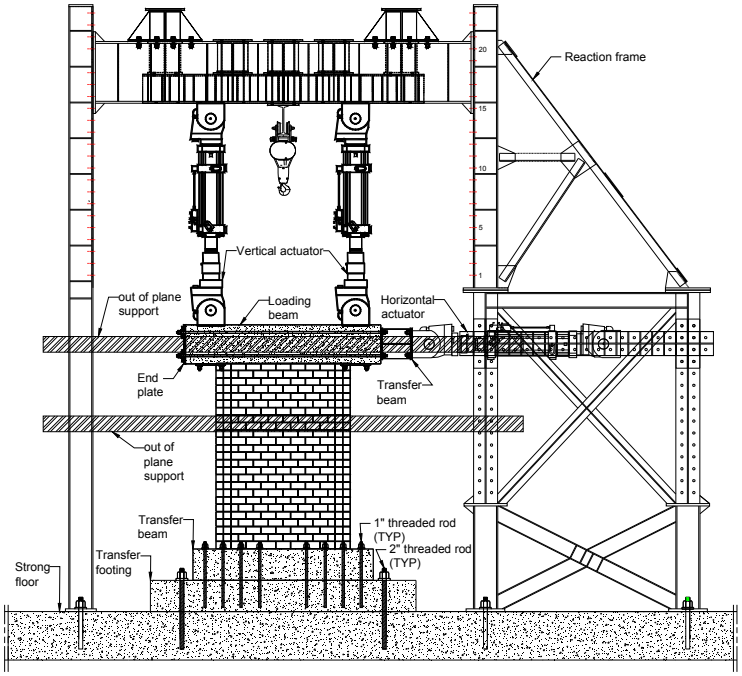

Figure 2: Test set-up

The horizontal actuator is used to apply the load at the center of the top loading beam. Two vertical actuators are used to apply the axial load and top moment to simulate the demanded moment induced from upper stories shear. The horizontal excitation was applied in a reversed cyclic pattern. Every two cycles are meant to achieve a specific target displacement, following the recommended loading protocol of ASTM E2126. Before reaching the wall's yielding point, yielding of the outermost vertical reinforcement, target displacements are applied as a fraction of the estimated yield displacement Δy (0.25Δy, 0.50Δy, 0.75 Δy). The remaining cycles were applied as multiple of the actual yield displacement (2Δy, 3Δy…) and repeated twice at each displacement level. The test was carried in sequential stages starting by applying the axial load by the two vertical actuators then the horizontal actuator moves until it reaches the required target displacement. Following that, the top moment was introduced through the vertical actuators according to the horizontal actuator load cell readings.

3 RESPONSE OF WALL 4 and Wall 5

3.1 Cracks and failure modes

For both walls, hair cracks appeared in the bed joints at $1\Delta_y$. The first visible cracks extended along the first storey height spaced at every two courses were observed at $3\Delta_y$ as horizontal flexural cracks in the

bed joints at the boundary elements and web areas. By increasing the applied loads more horizontal cracks developed at the bed joint in the boundary elements and the web area and in the zone between the bed joints, in the masonry block and the grouted core, in the boundary elements as shown in Figure 3.

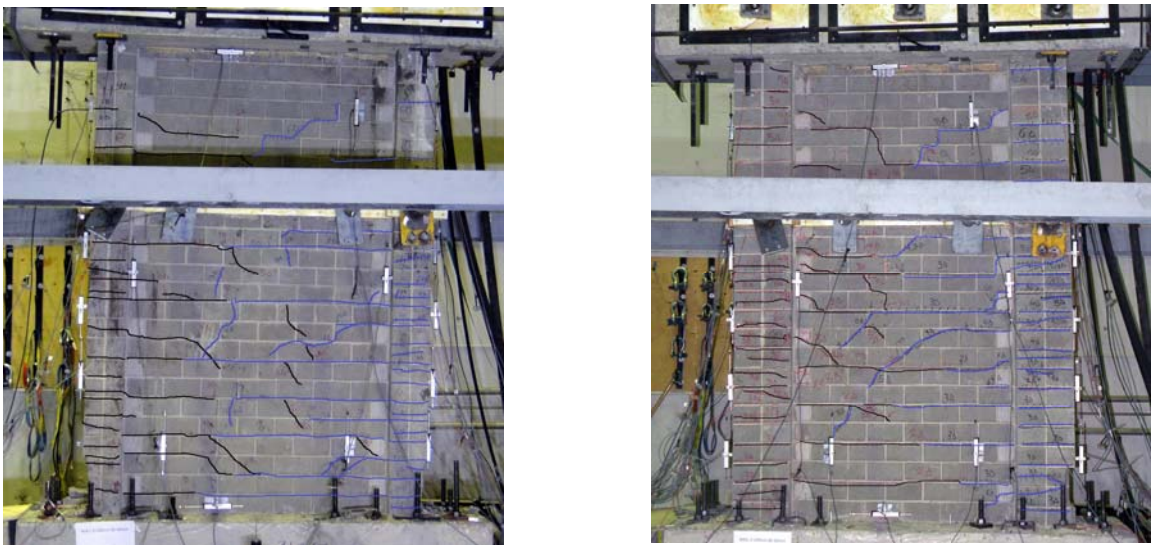

(a) (b)

Figure 3. Wall cracks: (a) Wall 4, (b) Wall 5

For wall 4, a vertical crack was observed between the grouted core and C-shape masonry unit in the toe area in the left boundary element along with crushing in the C-shape masonry unit face shell at $7\Delta_y$. The failure occurred at the second cycle of $13\Delta_y$ when buckling of vertical reinforcement and crushing of the grouted core took place as shown in Figure 4a. For wall 5, vertical cracks and crushing of boundary elements face shell at the toe zone took place at $9\Delta_y$. Vertical cracks in the boundary elements propagated till the 3rd course at $11\Delta_y$ as shown in Figure 4b. The failure occurred at the first push of $14\Delta_y$ when buckling of vertical reinforcement and crushing of the grouted core took place.

(a) (b)

Figure 4. Wall failure: (a) bar buckling and grout crushing in wall 4 at 13Δy, (b) vertical cracks in the boundary element in wall 5 at 11Δy.

3.2 Ultimate compressive strain

The relation between the average measured compressive strain at the wall's ends and the normalized measured lateral force for wall 4 and 5 is shown in Figure 5. The vertical displacements at the wall's ends were measured at 340 mm, 680 mm and 1020 mm segments height measured from the top of the wall footing. The discontinuity in the measurement was due to face shell spalling and losing the brackets that hold the potentiometers. The average measured compressive strains were 9.92×10^{-3} mm/mm and 13.15×10^{-3} mm/mm for wall 4 and wall 5 respectively. For both walls, the average measured compressive strain was at least four times the limit specified in CSA S304-14 standards. The maximum measured compressive strains were 17.65×10^{-3} mm/mm and 14.7×10^{-3} mm/mm for wall 4 and wall 5 respectively. Increasing the boundary element length reduced the measured compressive strain by 16.7%.

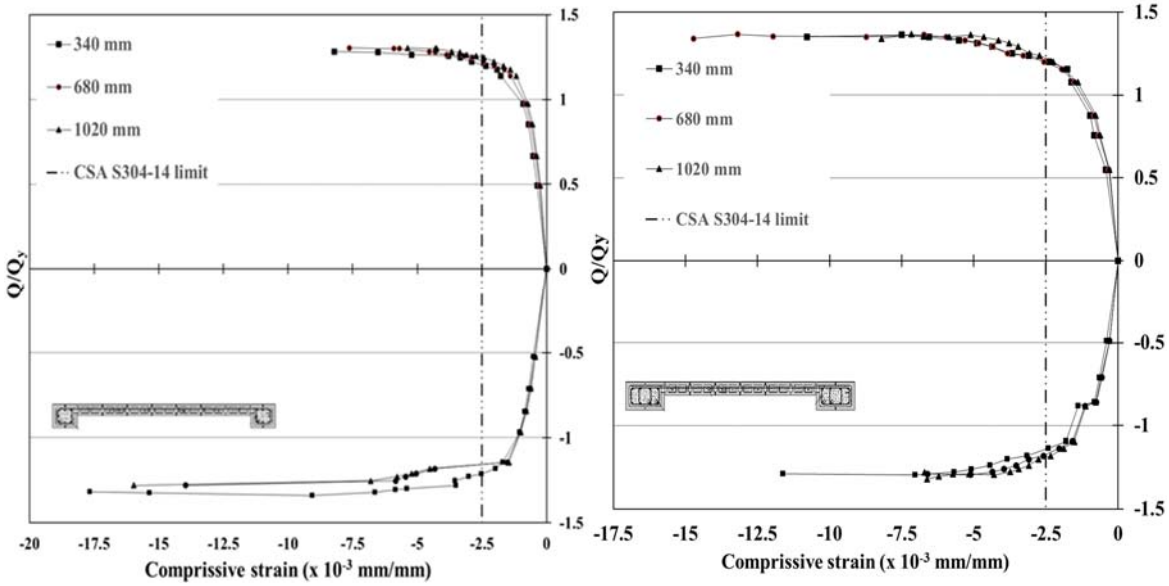

(a) (b)

Figure 5: Average compressive strain at 340 mm, 680 mm and 1020 mm segments height: a) for wall 4, b) for wall 5.

3.3 Load-deformation characteristics

The positive lateral force and displacement were measured in the push direction when the horizontal actuator pushes the wall to the west direction and vice versa. The wall's capacities are shown in Table 2 where Q_y is the measured yield lateral force and Q_u is the measured ultimate lateral force. The walls have a similar response in push and pull directions. The overstrength factor, Q_u/Q_y, for both walls is approximately 1.35.

Table 2. Wall's lateral strength

Wall	Q_y		Q_u		Q_u/Q_y	
	Push (kN)	Pull (kN)	Push (kN)	Pull (kN)	Push (%)	Pull (%)
Wall 4	56.69	-54.23	74.56	-74.09	131.52%	136.61%
Wall 5	56.37	-56.82	77.96	-74.95	138.30%	131.91%

The load-deformation relationship for wall 4 & 5 is shown in Figure 6 a& b. Both walls had the same yield and ultimate strength. Changing the boundary element length has almost no effect on the lateral resistance of the wall; however, wall 5 with longer boundary element has a ductility ratio of 14 compared with 13 for the wall with shorter boundary element, wall 4. This increase in the ductility could be explained as a result

of increasing the compressive strain in the long boundary elements wall, wall 5. The yield displacement will be taken as the displacement at the onset of yielding of the vertical reinforcement bars at the end of the wall. Since no force degradation was observed, the ultimate displacement will be considered as the maximum displacement recorded for the wall. Table 3 shows the measured yield and ultimate displacement and the displacement ductility ratio. From walls 4 and 5, increasing the boundary element length increased the average yield displacement by 7.14% and the ultimate displacement by 15.38%. Also, increasing the boundary element length increased the ductility ratio from 13 to 14 as shown in Table 3.

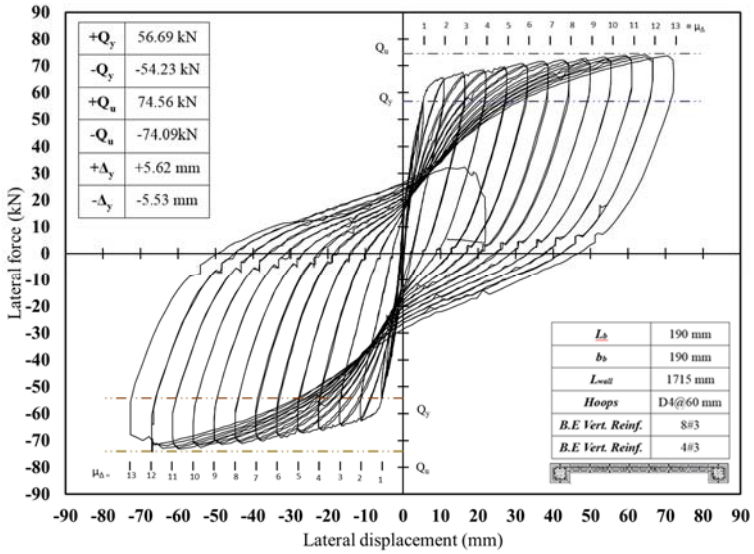

(a)

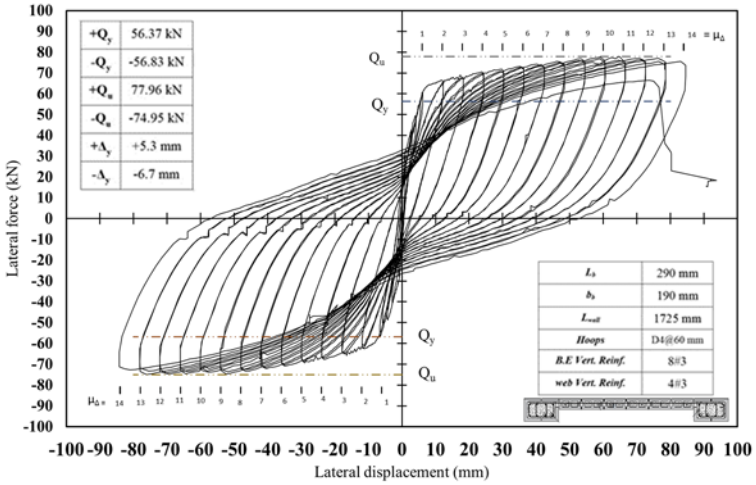

(b)

Figure 6: Load-deformation relationship: a) for wall 4, b) for wall 5.

The applied top moment was calculated based on Equation 1 were F_{VA} and F_{VB} are the forces in the vertical actuators and D is the horizontal distance between the vertical actuators.

$$[1]\ M_{top} = (F_{VA} + F_{VB})\frac{D}{2}$$

The forces in the vertical actuators were calculated on the basis of Equation 2 where F_H are the forces in the vertical actuator and horizontal actuator respectively, P is the applied axial load, h_{eff} is the wall's effective height, h_w is the specimen.

$$[2] F_V = \frac{P}{2} \pm \frac{h_{eff} - h_w}{D} F_H$$

Table 3. Measured yield and ultimate displacement.

Wall	Δ_y (mm)	Δ_u (mm)	μ_Δ
Wall 4	5.6	72.8	13
Wall 5	6	84	14

3.4 Energy dissipation

The relationship between the normalized dissipated energy and the ductility ratio is shown in Figure 7. Normalized dissipated energy was taken as the ratio between the amount of energy dissipated at each ductility level and the energy dissipated at yield. The amount of dissipated energy for each cycle was taken as the area bounded by the load-deformation curve. Wall 5 found to be able to dissipate more energy rather than wall 4 by 32% due to the increase in the number of cycles. However, the amount of energy dissipated by each cycle is higher in wall 4 due to shifting the vertical reinforcement in wall 4 toward the wall's ends compared to wall 5. The results are conforming with Kapoi (2012) results which concluded that walls with concentrated reinforcement found to dissipate 50% more energy.

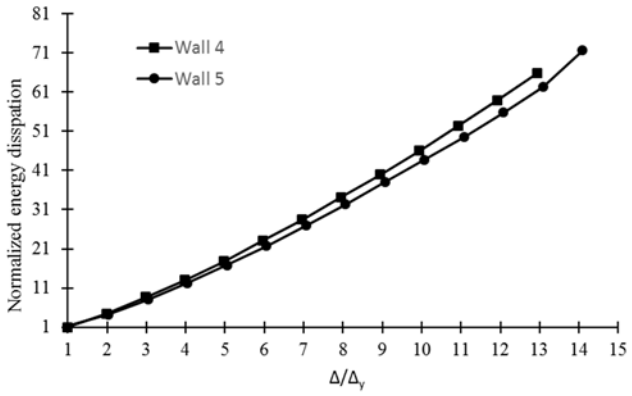

Figure 7: Normalized energy dissipation- ductility ratio relationship

3.5 Damping ratio

Damping ratio, ξ, was calculated using Equation 1 where E_{Diss} is the dissipated at a certain level of ductility and E_{sto} is the elastic strain energy stored in an equivalent linear elastic system (Elnashai, Amr S. 2008).

$$[1]\ \xi = \frac{1}{4\pi}\left(\frac{E_{Diss}}{E_{sto}}\right)$$

As shown in Figure 8, the hysteresis damping is increasing with the increase of the ductility level for both walls. In general, the hysteresis damping values in wall 4 are higher than wall 5. At ductility level equable to one, both walls have almost the same damping ratio, 6%. With the increase in the ductility ratio, the damping ratio increased with a higher rate in wall 4.

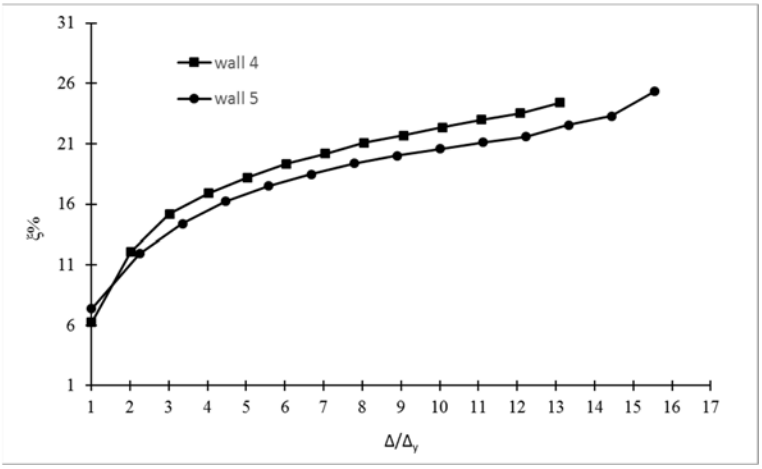

Figure 8: Hysteresis damping ratio-ductility ratio relationship

4 CONCLUSIONS

The boundary elements in the previously tested walls were constructed using regular stretcher blocks. Using regular stretcher blocks caused some limitations due to the geometry restrictions of the stretcher units. New C-shape boundary element blocks were utilized in wall's boundary elements allowing various lateral reinforcement spacing, increase the vertical reinforcement and increase the boundary element size. The test setup is adequate and is capable of simulating the test for the lower panel of RMSW in 10 storey building. One of the advantages of using C-shaped masonry units to form the boundary elements that gives the flexibility to change the shape and the size of the boundary element. Wall 4 and wall 5 were designed to have the same lateral resistance to investigate the effect of changing the boundary element size on the wall's failure mode, the measured ultimate compressive strain, load-deformation characteristics, energy dissipation and damping ratio of the masonry shear wall. Both walls were designed to have almost the same total length and the lateral capacity. The maximum measured compressive strains were 17.65×10^{-3} mm/mm and 14.7×10^{-3} mm/mm for wall 4 and wall 5 respectively. Increasing the boundary element length reduced the measured compressive strain by 16.7%. Wall 5 with larger boundary elements has better ductility ratio and deformation capacity. However, wall 4 with a smaller boundary element has better damping and energy dissipation than wall 5. In general, the differences in the behaviour between the two walls is not big. However, the results showed that the engineer has the option to use either wall depends on his needs. For example, walls with large boundary elements can carry more axial load, compared with walls with the same length, and still provide good ductility with a small sacrifice in the amount of the dissipated energy.

5 ACKNOWLEDGEMENTS

The authors acknowledge the support from the Natural Science and Engineering Research Council of Canada (NSERC), l'Association des Entrepreneurs en Maçonnerie du Québec (AEMQ), the Canadian Concrete Masonry Producers Association (CCMPA) and Canada Masonry Design Centre (CMDC).

6 REFERENCES

Banting, Bennett R., and Wael W. El-Dakhakhni. 2012. "Force- and Displacement-Based Seismic Performance Parameters for Reinforced Masonry Structural Walls with Boundary Elements." *Journal of Structural Engineering* **138** (12): 1477-1491

Canadian Commission on Building and Fire Codes. 2015. *National Building Code of Canada 2015*. Vol. 1. National Research Council of Canada.

CSA S304-14. 2014. "Design of Masonry Structures." *CSA Group*. Mississauga, Ontario: CSA Group. doi:10.1080/09613218309442127.

Elnashai, Amr S., and Luigi Di Sarno. 2008. *Fundamentals of Earthquake Engineering*. New York: Wiley.

Kapoi, Christina Marie. 2012. “Experimental Performance of Concrete Masonry Shear Walls under In-Plane Loading.” Washington State University.

Oh, Young-hun, Sang Whan Han, and Li-Hyung Lee. 2002. “Effect of Boundary Element Details on the Seismic Deformation Capacity of Structural Walls.” Earthquake Engineering And Structural Dynamics **31**: 1583-1602.

Robazza, B, K J Elwood, D L Anderson, and S Brzev. 2013. “In-Plane Seismic Behaviour of Slender Reinforced Masonry Shear Walls : Experimental Results.” In *12th Canadian Masonry Symposium*. Vol. **2010**. Vancouver, British Columbia: 12th Canadian Masonry Symposium.

Shedid M. T., Dakhakhni, W.W., and Drysdale R. G. 2010. “Characteristics of Rectangular, Flanged, and End-Confined Reinforced Concrete Masonry Shear Walls for Seismic Design.” *Journal of Structural Engineering* **136** (12): 1471-1482